

Article

Mesoporous WN/WO₃-Composite Nanosheets for the Chemiresistive Detection of NO₂ at Room Temperature

Fengdong Qu ¹, Bo He ¹, Rohiverth Guarecuco ² and Minghui Yang ^{1,*}

¹ Dalian Institute of Chemical Physics, Chinese Academy of Sciences, Dalian 116023, China; qufd@dicp.ac.cn (F.Q.); hebomk@dicp.ac.cn (B.H.)

² Department of Chemical Engineering, Massachusetts Institute of Technology, Cambridge, MA 02139-4307, USA; rog2029@med.cornell.edu

* Correspondence: myang@dicp.ac.cn; Tel.: +86-411-8246-3026

Academic Editor: Rainer Niewa

Received: 13 June 2016; Accepted: 21 July 2016; Published: 26 July 2016

Abstract: Composite materials, which can optimally use the advantages of different materials, have been studied extensively. Herein, hybrid tungsten nitride and oxide (WN/WO₃) composites were prepared through a simple aqueous solution route followed by nitriding in NH₃, for application as novel sensing materials. We found that the introduction of WN can improve the electrical properties of the composites, thus improving the gas sensing properties of the composites when compared with bare WO₃. The highest sensing response was up to 21.3 for 100 ppb NO₂ with a fast response time of ~50 s at room temperature, and the low detection limit was 1.28 ppb, which is far below the level that is immediately dangerous to life or health (IDLH) values (NO₂: 20 ppm) defined by the U.S. National Institute for Occupational Safety and Health (NIOSH). In addition, the composites successfully lower the optimum temperature of WO₃ from 300 °C to room temperature, and the composites-based sensor presents good long-term stability for NO₂ of 100 ppb. Furthermore, a possible sensing mechanism is proposed.

Keywords: WN/WO₃ composite; nanosheets; gas sensor; NO₂; room temperature

1. Introduction

Gas sensors have been in increasing demand in recent years because of their wide applications, not only in environmental monitoring, but also in human health [1–4]. Metal oxide semiconductors (MOSs) based gas sensors have been intensely investigated for their high sensitivity, excellent selectivity, good portability, and low cost [5–7]. However, for detecting lower concentrations of toxic and disease signal gases, composite materials have shown greater potential than bare materials which exhibit low or no sensitivity in low gas concentrations (sub-ppm), as well as poor selectivity [8,9]. These composite materials include heterostructural materials, doped materials, and noble metal decorated materials, among which the heterostructural materials have been widely investigated because of super injection of carriers [10,11]. When different materials hybridize to form a heterojunction, an electron depletion layer (EDL) or an electron accumulation layer (EAL) will form at the interfaces. It is well acknowledged that the heterojunctions can serve as a lever in electron transfer, which can facilitate or restrain the electron transfer, resulting in enhanced sensing performance of a gas sensor [12]. Thus, designing composite sensing materials with heterostructures is regarded as one of the best strategies to achieve excellent gas sensing characteristics.

In the past few years, various sensing materials have been prepared that have exhibited excellent gas sensing characteristics [13,14]. However, to date and to the best of our knowledge, there have

been very scarce reports about heterostructural metal nitride and oxide composites for sensing applications [15]. Metal nitrides can have varied properties: from metal-like, to semiconducting, to that of insulators. Thus, introducing metal nitrides into metal oxides could tune electrical properties that have great influence on gas sensing characteristics, such as carrier mobility and electrical resistivity [16]. In addition, other reports have demonstrated that establishing heterojunction could largely decrease the working temperature of sensing materials [17–19]. Thus, designing composites consisting of metal nitrides and oxides, and innovatively applying the composites as gas sensor materials, is of vital significance.

Tungsten trioxide (WO_3) is a multifunctional material that has been widely investigated as a photocatalyst [20,21] and a gas sensor [22,23]. When applied as a gas sensing material, WO_3 exhibits sensitivity to several gases, and has especially high-sensitivity to NO_2 , making it an ideal material for detecting NO_2 [23–25]. However, because of its wide band gap, (2.5–3.5 eV) WO_3 -based sensors have to work at high working temperature or with the assistance of ultraviolet light [19,26,27]. Therefore, efforts should be focused on lowering working temperature while achieving optimal sensitivity. Tungsten nitride (WN) shows metallic properties with a resistivity of $10.9 \times 10^{-5} \Omega \cdot \text{m}$ at room temperature [28]. Therefore, synthesis of WN-composite WO_3 materials for detecting NO_2 gas at low working temperature may be feasible and is highly desirable.

Herein, for the first time, we present an applicable strategy for the efficient synthesis of new gas sensing materials made of hybrid WN/ WO_3 composites. The strategy includes the synthesis of a porous WO_3 nanosheets precursor and subsequent transformation to WN/ WO_3 composites by thermal annealing of the as-prepared precursor in NH_3 . The WN/ WO_3 composites sensing materials exhibit sensitive, selective and reliable detection of NO_2 at room temperature.

2. Results and Discussion

2.1. Structure, Composition and Morphology

Powder X-ray diffraction (XRD) was used to characterize the phase composition and purity of the as-synthesized products. The yellow powder (precursors) obtained from the oil bath reaction agreed well with reported orthorhombic tungsten oxide hydrate ($\text{WO}_3 \cdot \text{H}_2\text{O}$, JCPDS No. 84-0886), as shown in Figure 1a (Pattern A) [29]. The $\text{WO}_3 \cdot \text{H}_2\text{O}$ precursors were converted into WN and WN/ WO_3 composites by nitridation in NH_3 atmosphere and oxidation in air, under heat treatment at 700°C and 200°C for 3 h, respectively. Figure 1a (Patterns B and C) shows the XRD of WN and WN/ WO_3 composites. As shown in pattern b, all the diffraction peaks matched well with those of hexagonal WN (JCPDS No. 65-2898). For the composite (Pattern C), the crystal phase was a mixture of hexagonal WN (JCPDS No. 65-2898), a big convex appearing in the position of 2θ 20° – 30° , and a small convex in the position of 2θ 50° – 60° , which can be attributed to amorphous WO_3 . Thus, the final product is a composite material composed of hexagonal WN and amorphous WO_3 (WN/ WO_3). The composites underwent a mass change during the transformation from WN to WO_3 by calcination in air. By using this mass change, we can calculate the ratio of WN to WO_3 . Thermogravimetric analyses of the products at temperature range of 0 – 1000°C are shown in Figure 1b. The DSC-TGA results of the WN/ WO_3 composite nanosheets are displayed in Figure 1b. It was observed from the TGA curve that the specimen shows a weight loss of about 1%, which relates to adsorbed water and other trace substances. When the temperature reached about 211.5°C , the weight of the specimen began to increase. When the temperature reaches about 457°C , the weight nearly reaches stability. Moreover, the DSC curve exhibited an obvious exothermal peak at 426°C , which corresponded to the obvious weight gain of approximately 8.86% between 211 and 457°C in the TGA curves. The significant weight gain was attributed to the reaction of the WN with oxygen to generate WO_3 . According to the weight gain of approximately 8.86%, the WN content of the composites is calculated to be 55.9%.

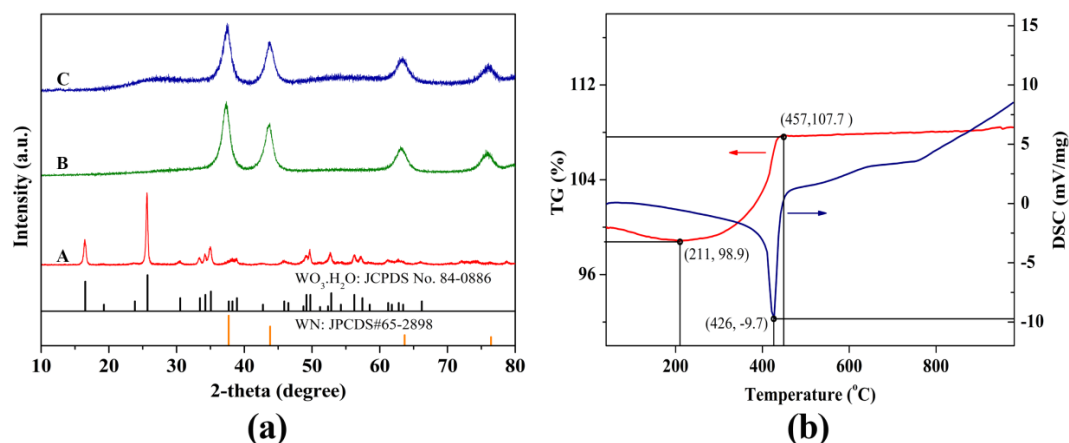


Figure 1. (a) Powder X-ray diffraction (XRD) patterns of tungsten oxide hydrate ($\text{WO}_3 \cdot \text{H}_2\text{O}$) A, tungsten nitride (WN) B and hybrid tungsten nitride and oxide (WN/ WO_3) composites C; (b) differential scanning calorimetry-thermal gravimetric analysis (DSC-TGA) curves of WN/ WO_3 composites.

The morphology of WN/ WO_3 composites was characterized through SEM and TEM analysis, and the results are shown in Figure 2. According to Figure 2a–c, the WN/ WO_3 composites exhibited square shaped nanosheets with uniform lateral dimensions mainly ranging from 80 to 150 nm (Figure 2a,b) and thickness of 10 to 30 nm (Figure 2c). In addition, relatively homogeneous pores with average diameter of 10 nm were dispersed uniformly at the surfaces of WN/ WO_3 composites. The porous feature may have contributed to the volume shrinkage caused by transformation of orthorhombic $\text{WO}_3 \cdot \text{H}_2\text{O}$ to hexagonal WN. Figure 2d shows the HRTEM image of the WN/ WO_3 composites, where the lattice fringes d-spacings of 0.239 and 0.204 nm are identified and correspond to the (111) and (200) planes of hexagonal WN (JCPDS No. 65-2898), respectively. The inset of Figure 2d presents the selected area electron diffraction (SEAD) of WN/ WO_3 composites. The distinctive diffraction rings and spots on the SEAD pattern match the crystal structure identification obtained from the HRTEM and XRD. The diffraction rings are indexed to cubic WN (JCPDS No. 65-2898) (111), (200), (220), (311), (400), and (331) planes, respectively.

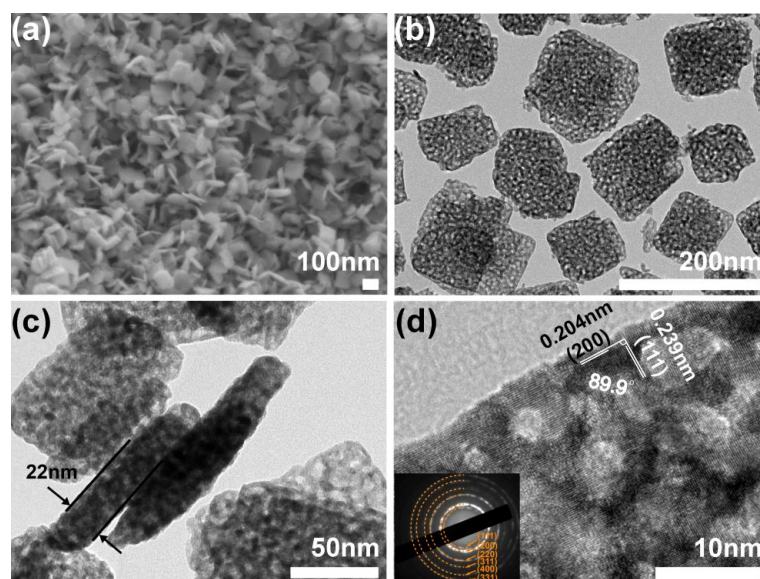


Figure 2. SEM images (a); top/side-view transmission electron microscopy (TEM) images (b–c); and high-resolution transmission electron microscopy (HRTEM) images of WN/ WO_3 composites (d). Inset: selected area electron diffraction (SEAD) pattern of WN/ WO_3 composites.

2.2. Gas Sensing Characteristics

Dynamic sensing performance of WN/WO₃ composites-based sensors to various concentrations of NO₂ at room temperature is shown in Figure 3a. NO₂ is an oxidizing gas, so when an NO₂ molecule adsorbs on the surface of WN/WO₃ composites, it captures electrons from the composites, resulting in the increase of resistance of the composites-based sensors upon exposure to NO₂. Figure 3b plots the sensor response as a function of NO₂ concentration, and shows that with an increase in NO₂ concentration, the response of the sensor also exhibits an increasing trend. Interestingly, the sensitivities to NO₂ concentrations from 5 to 100 ppb and 100 to 1000 ppb exhibit linear dependence, fitting well into two linear curves which have different slopes. It is well understood that electrical conductance shows strong dependence on carrier and mobility ($\sigma = ne\mu_n$, where n is the concentration of electrons, e is electronic charge, and μ_n is electron mobility), and that electrical resistivity is the reciprocal of electrical conductance. When the WN/WO₃ composites sensor is exposed to low concentration of NO₂, the amount of adsorbed NO₂ is so sparse that the degradation of carrier could be almost negligible, and the response of the sensor exhibits a “high increase model”. However, when exposed to high concentration of NO₂, the effect of NO₂ adsorption will be enhanced, and the degradation of carrier mobility becomes relatively remarkable, resulting in a decrease in the rate of sensitivity increase under abundant NO₂ adsorption [30]. The detection limit of the WN/WO₃ composites sensor for NO₂ is calculated to be approximately 1.28 ppb based on signal-to-noise ratio of 3 (see the Section “Calculation of Theoretical Limit of Detection Using Signal/Noise Ratio” in Supplementary Materials), which is far below the immediately dangerous to life or health (IDLH) values (NO₂: 20 ppm) defined by the U.S. National Institute for Occupational Safety and Health (NIOSH). The recommended NO₂ exposure limit defined by the NIOSH is 1 ppm [31].

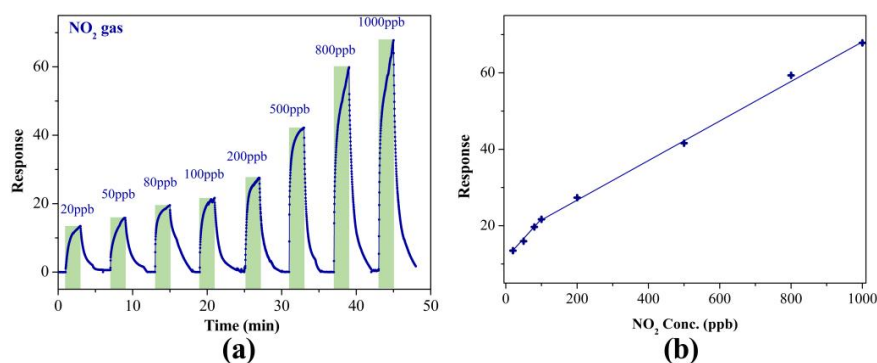


Figure 3. (a) Dynamic sensing performance of WN/WO₃ composites sensor to NO₂ with concentration from 20 to 1000 ppb at room temperature (RT); (b) calibration curves of WN/WO₃ composites sensor towards various concentrations of NO₂ at RT.

Selective detection of target gas from various interference gases is still an unsolved drawback for chemiresistive gas sensors [32]. The responses of the sensor based on WN/WO₃ composites to common vehicle exhaust, including SO₂, CO₂, moisture, CO, NH₃, ethanol and NO₂, were measured to quantify the selectivity, which is shown in Figure 4. As clearly illustrated in Figure 4, the sensor shows a high response to NO₂, which is more than 2 times higher than that for other interference gases, indicating the excellent selectivity to NO₂ as opposed to other selected interference gases. The selective detection to NO₂ gas might be due to the high reactivity and large electron affinity (2.28 eV) of NO₂, in comparison with pre-adsorbed oxygen (0.43 eV) and other test gases [33]. In addition, the responses of the sensor based on WN/WO₃ composites to 200 ppb NO₂ at RT under different humidities were tested and the result is shown in Figure S1. It can be observed that, with increasing relative humidity, the response of the sensor decreases because of the competition between water molecules and NO₂ molecules for the reacting sites [34]. However, the sensor shows a high response of 17.8 even at high humidity of 90 RH%.

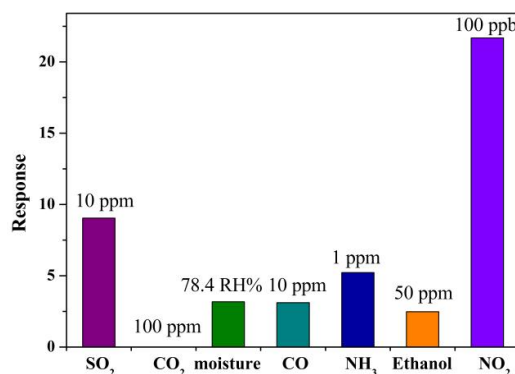


Figure 4. Cross-response of WN/WO₃ composites sensor to various gases.

Figure 5a shows the response and recovery times of the WN/WO₃ composites-based sensor. With increasing NO₂ concentration, the response time and recovery time both experience a decrease. The reason why the response and recovery times are substantially longer at low concentration is unclear and needs further study. The following can be considered as a plausible explanation. At low concentration of ambient NO₂, the NO₂ molecules occupy a lower percentage of air relative to oxygen molecules, so the probability of NO₂ molecules arriving and being captured by the surface of the sensing materials (WN/WO₃) is relatively smaller, resulting in a long response. When the concentration of NO₂ increases, the probability of NO₂ molecules arriving and being captured by the surface of sensing materials becomes higher, decreasing the response time. As for the recovery time: at low concentration of NO₂, the amount of adsorbed NO₂ is too small, making it difficult to desorb completely, resulting in a relatively longer recovery time. When the concentration is higher, the concentration difference between the surface of WN/WO₃ and ambient atmosphere is large enough to desorb NO₂ molecules quickly, reducing the recovery time. Similar observations have also been reported by other investigators [35,36]. In addition, the sensor shows excellent reversibility properties with a response time of less than 80 s and a recovery time of less than 180 s, regardless of the NO₂ concentration. Stability is another key quality indicator in the development of gas sensors for real markets. Thus, we measured the response of the WN/WO₃ composites-based sensor for 7 weeks, once a day (every 24 h) at room temperature for a week and then once a week for 6 weeks, shown in Figure 5b. We can observe that the sensor experiences a loss in response of less than 12.27% after 7 weeks of aging. The response of the sensor comes into saturation after 2 weeks. The results indicate that the WN/WO₃ composites sensor exhibits good long-term stability.

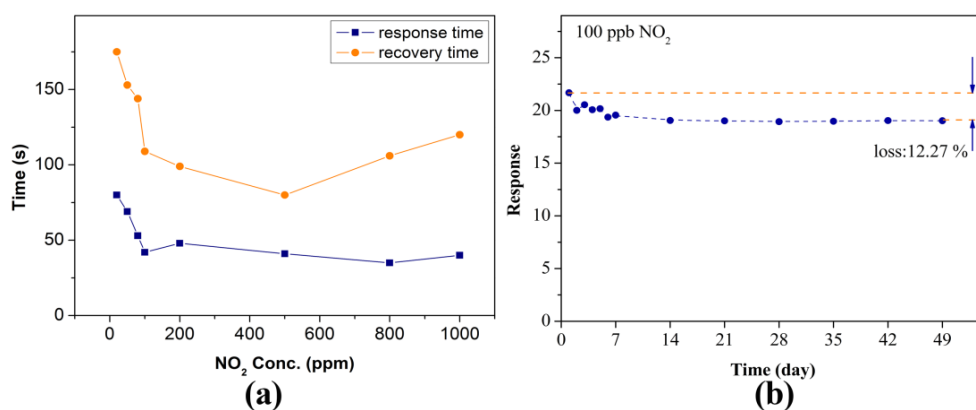


Figure 5. (a) Response and recovery time of WN/WO₃ composites sensor to various concentrations of NO₂ at RT. (b) Stability measurement of the WN/WO₃ composites sensor to 100 ppb NO₂ at RT for 7 weeks.

Dynamic sensing transients of WN/WO₃ composites and WO₃ nanosheets to 100 ppb NO₂, at room temperature and 300 °C (the optimum working temperature of WO₃, data shown in Figure S2) respectively, are shown in Figure 6. It can be observed that the R_a of WN/WO₃ composites is lower than that of WO₃ nanosheets, which confirms that the introduction of WN into WO₃ can decrease the resistance of the materials. In addition, the responses of WN/WO₃ composites and WO₃ nanosheets sensors to 100 ppb NO₂ were 23.7 and 6.2, respectively, which suggests that gas sensing responses towards NO₂ can be enhanced by partial nitrogenizing of WO₃. Furthermore, the introduction of WN into WO₃ apparently decreases the working temperature from 300 °C to room temperature.

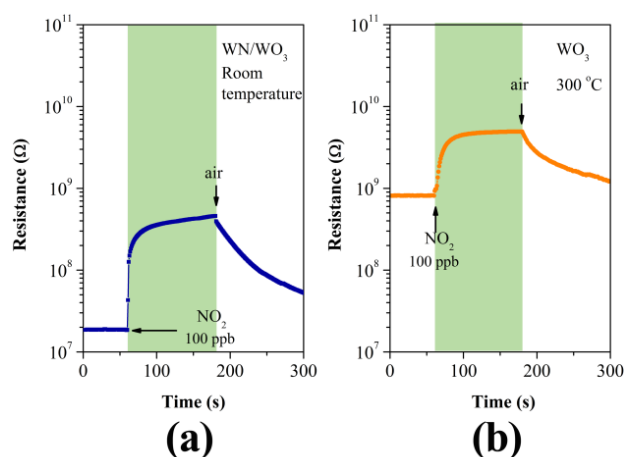
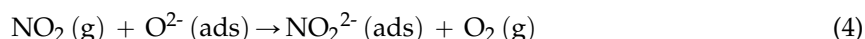


Figure 6. Dynamic sensing transients to 100 ppb NO₂ of (a) WN/WO₃ composite nanosheets sensors at room temperature; and (b) WO₃ nanosheets sensors at 300 °C.

2.3. Gas Sensing Mechanism

Typically, the gas sensing mechanism of WO₃ belongs to surface-controlled type, where the adsorption and desorption of NO₂ molecules on the surface of WO₃ play a vital role [24]. In ambient air, the oxygen molecules will adsorb on the surface of WO₃ and trap electrons from the conduction band of WO₃ to form ionic oxygen species (O²⁻, O⁻ and O²⁻), decreasing the electron concentration of the surface of WO₃, resulting in a high-resistance depletion layer at the surface [37]. When the NO₂ gases come in, the NO₂ molecules, which are highly electrophilic, will capture electrons from the conduction band of WO₃, and will also react with the adsorbed ionic oxygen species. This will lead to a further decrease in electron concentration, increasing the resistance of WO₃. The reactions taking place on the surface of WO₃ are as follows.



The as-fabricated WN/WO₃ composites-based sensor, when compared with WO₃ sensor, exhibited enhanced sensing performances. The reasons why WN/WO₃ composites-based sensor shows enhanced gas sensing characteristics are still unclear and worthy of further investigation. The following can be considered as a plausible explanation based on our experimental results. Firstly, WN exhibits metallic properties with a high electron concentration of about $(5-6) \times 10^{20} \text{ cm}^{-3}$ and a resistivity of $(1-2) \times 10^{-1} \Omega$ at room temperature [38]. However, WO₃ is an n-type semiconductor, whose resistivity is far larger than that of WN. Thus, the electrons will transfer from the high concentration side to the low concentration side because of diffusion effect, resulting in a lower resistivity of the composites when

compared with bare WO₃. The lower baseline of resistivity of WN/WO₃ composites will eventually increase the response ($S = (R_g/R_a - 1) \times 100\%$) of the sensor. In addition, WN and WO₃ themselves did not show any sensing properties for NO₂ at room temperature (Figure S3). However, the WN/WO₃ composites exhibit excellent sensing characteristics to NO₂ at room temperature. This may largely prove that there might be some synergetic effect in our WN/WO₃ composites, leading to room temperature sensing for NO₂.

3. Materials and Methods

3.1. Materials

Sodium tungstate dihydrate (Na₂WO₄·2H₂O, AR) of ≥99.5% purity was purchased from Aladdin Chemical Reagent Co., Ltd. (Shanghai, China). Hydrochloric acid (HCl) and oxalic dihydrate (H₂C₂O₄·2H₂O) of analytical reagent grade were purchased from Sinopharm Chemical Reagent Co., Ltd. (Shanghai, China).

3.2. Synthesis

Na₂WO₄·2H₂O (3.2985 g, 0.01 mol) was dissolved in 50 mL deionized water with continuous stirring for 30 min at room temperature. 50 mL of HCl aqueous solution (2 M) was added dropwise into the above solution under continuous stirring. A certain amount of H₂C₂O₄·2H₂O, with a mole ratio of 0.25 Na₂WO₄·2H₂O to H₂C₂O₄·2H₂O, was then added into the above system. The reaction vessel was then transferred to a 90 °C oil bath for 3 h. The yellow precipitate obtained was filtered and washed with deionized water and absolute ethanol several times, and subsequently dried at 60 °C in a vacuum oven for 24 h. Then, the yellow powder was nitrided at 700 °C at a ramp rate of 10 °C·min⁻¹ under NH₃ gas flow rate of 300 sccm (standard-state cubic centimeter per minute) for 3 h. Finally, the nitride was calcined at 420 °C in air for 3 h at a ramp rate of 10 °C·min⁻¹.

3.3. Materials Characterizations

X-ray diffraction (XRD) analysis was conducted on a Rigaku MiniFlex 600 powder X-ray diffractometer (Rigaku Corporation, Tokyo, Japan) with Cu Kα radiation ($\lambda = 1.5418 \text{ \AA}$, accelerating voltage 40 kV, applied current 15 mA) at scanning rate of 1 °/min. Scanning electron microscopy (SEM) images were performed on a JSM-7800F (Japan Electron Optics Laboratory Co., Ltd., Tokyo, Japan) instrument (accelerating voltage 3.0 kV). Transmission electron microscopy (TEM) and high-resolution transmission electron microscopy (HRTEM) observations were conducted on an FEI TecnaiG2 F30 (Japan Electron Optics Laboratory Co., Ltd.). Differential Scanning Calorimetry (DSC) and thermal gravimetric analysis (TGA) were done on a NETZSCH/STA 449 F1 (Netzsch, Selb, Freistaat Bayern, Germany).

3.4. Fabrication and Measurement of Gas Sensor

Typically, 50 mg·mL⁻¹ WN/WO₃ composites-ethanol solution was deposited on the surface of the device and calcined at 100 °C for 3 h. Gas sensing performances were measured by a homemade sensor testing system (a cylindrical glass chamber with a volume of 100 mL). A gas mixing line equipped with mass flow controllers was designed to prepare target gases at specific concentrations in the testing chamber as shown in Figure S4. The resistance changes of sensor in air or tested gas were monitored by a high-resistance meter (Victor, 86E, Shenzhen, China). The response value (S) was defined as $S = (|R_g - R_a| / R_a) \times 100\%$, where R_a and R_g denoted the resistance of the sensors in the absence and presence of the target gases (reducing gases), respectively. The time taken by the sensor to achieve 90% of the total resistance change was defined as the response time in the case of response (target gas adsorption) or the recovery time in the case of recovery (target gas desorption).

4. Conclusions

In conclusion, we successfully synthesized WN/WO₃ composites through a simple strategy, and innovatively utilized them as gas sensing materials. The WN/WO₃ composites-based sensor exhibited sensitivity and high selectivity to NO₂ at room temperature. Overall, the excellent NO₂ sensing performance of the WN/WO₃ composites-based sensor supplies exciting opportunities for environmental monitoring and disease diagnosing. Furthermore, we expect our findings to bring up new promising gas sensing materials, and to inspire rational synthesis of other transition metal nitride and oxide hybrids for high-performance gas sensing.

Supplementary Materials: The following are available online at www.mdpi.com/2304-6740/4/3/24/s1, Figure S1: Response of WN/WO₃ composites sensor at RT upon exposure to 200 ppb NO₂ concentration at various relative humidities (RH), Figure S2: Response of the sensor based on WO₃ nanosheets to 100 ppb NO₂ as a function of the operating temperature, Figure S3: Resistances of the sensors based on WN and WO₃ to 100 ppb NO₂ at room temperature, Calculation of theoretical limit of detection using signal/noise ratio, Figure S4: The schematic illustration of (a) gas sensing analysis system and (b) gas mixing line equipment.

Acknowledgments: This work is supported by National Natural Science Foundation of China through grant 21471147 and Liaoning Provincial Natural Science Foundation through grant 2014020087. Minghui Yang would like to thank the National “Thousand Youth Talents” program of China.

Author Contributions: The preparation of the manuscript was made by all authors. Fengdong Qu and Minghui Yang conceived and designed the experiments; Fengdong Qu and Bo He performed the experiments; Fengdong Qu, Bo He and Rohiverth Guarecuco analyzed the data.

Conflicts of Interest: The authors declare no conflict of interest.

References

1. Haick, H.; Broza, Y.Y.; Mochalski, P.; Ruzsanyi, V.; Amann, A. Assessment, origin, and implementation of breath volatile cancer markers. *Chem. Soc. Rev.* **2014**, *43*, 1423–1449. [[CrossRef](#)]
2. Hagleitner, C.; Hierlemann, A.; Lange, D.; Kummer, A.; Kerness, N.; Brand, O.; Baltes, H. Smart single-chip gas sensor microsystem. *Nature* **2001**, *414*, 293–296. [[CrossRef](#)] [[PubMed](#)]
3. Peng, G.; Tisch, U.; Adams, O.; Hakim, M.; Shehada, N.; Broza, Y.Y.; Billan, S.; Abdah-Bortnyak, R.; Kuten, A.; Haick, H. Diagnosing lung cancer in exhaled breath using gold nanoparticles. *Nat. Nanotechnol.* **2009**, *4*, 669–673. [[CrossRef](#)] [[PubMed](#)]
4. Kolmakov, A.; Klenov, D.; Lilach, Y.; Stemmer, S.; Moskovits, M. Enhanced gas sensing by individual SnO₂ nanowires and nanobelts functionalized with Pd catalyst particles. *Nano Lett.* **2005**, *5*, 667–673. [[CrossRef](#)] [[PubMed](#)]
5. Deng, S.; Tjoa, V.; Fan, H.M.; Tan, H.R.; Sayle, D.C.; Olivo, M.; Mhaisalkar, S.; Wei, J.; Sow, C.H. Reduced graphene oxide conjugated Cu₂O nanowire mesocrystals for high-performance NO₂ gas sensor. *J. Am. Chem. Soc.* **2012**, *134*, 4905–4917. [[CrossRef](#)] [[PubMed](#)]
6. Rai, P.; Khan, R.; Raj, S.; Majhi, S.M.; Park, K.-K.; Yu, Y.-T.; Lee, I.-H.; Sekhar, P.K. Au@Cu₂O core-shell nanoparticles as chemiresistors for gas sensor applications: Effect of potential barrier modulation on the sensing performance. *Nanoscale* **2014**, *6*, 581–588. [[CrossRef](#)] [[PubMed](#)]
7. Jing, Z.; Zhan, J. Fabrication and gas-sensing properties of porous ZnO nanoplates. *Adv. Mater.* **2008**, *20*, 4547–4551. [[CrossRef](#)]
8. Cheng, W.; Ju, Y.; Payamyar, P.; Primc, D.; Rao, J.; Willa, C.; Koziej, D.; Niederberger, M. Large-area alignment of tungsten oxide nanowires over flat and patterned substrates for room-temperature gas sensing. *Angew. Chem. Int. Ed.* **2015**, *54*, 340–344. [[CrossRef](#)] [[PubMed](#)]
9. Kim, H.W.; Na, H.G.; Kwon, Y.J.; Cho, H.Y.; Lee, C. Decoration of Co nanoparticles on ZnO-branched SnO₂ nanowires to enhance gas sensing. *Sens. Actuators B Chem.* **2015**, *219*, 22–29. [[CrossRef](#)]
10. Liang, Y.; Cui, Z.; Zhu, S.; Li, Z.; Yang, X.; Chen, Y.; Ma, J. Design of a highly sensitive ethanol sensor using a nano-coaxial p-Co₃O₄/n-TiO₂ heterojunction synthesized at low temperature. *Nanoscale* **2013**, *5*, 10916–10926. [[CrossRef](#)] [[PubMed](#)]
11. Xu, S.; Gao, J.; Wang, L.; Kan, K.; Xie, Y.; Shen, P.; Li, L.; Shi, K. Role of the heterojunctions in In₂O₃-composite SnO₂ nanorod sensors and their remarkable gas-sensing performance for NO_x at room temperature. *Nanoscale* **2015**, *7*, 14643–14651. [[CrossRef](#)] [[PubMed](#)]

12. Zhou, X.; Feng, W.; Wang, C.; Hu, X.; Li, X.; Sun, P.; Shimanoe, K.; Yamazoe, N.; Lu, G. Porous ZnO/ZnCo₂O₄ hollow spheres: Synthesis, characterization, and applications in gas sensing. *J. Mater. Chem. A* **2014**, *2*, 17683–17690. [[CrossRef](#)]
13. Sun, P.; Zhou, X.; Wang, C.; Shimanoe, K.; Lu, G.; Yamazoe, N. Hollow SnO₂/α-Fe₂O₃ spheres with a double-shell structure for gas sensors. *J. Mater. Chem. A* **2014**, *2*, 1302–1308. [[CrossRef](#)]
14. Chan, N.Y.; Zhao, M.; Wang, N.; Au, K.; Wang, J.; Chan, L.W.H.; Dai, J. Palladium nanoparticle enhanced giant photoresponse at LaAlO₃/SrTiO₃ two-dimensional electron gas heterostructures. *ACS Nano* **2013**, *7*, 8673–8679. [[CrossRef](#)] [[PubMed](#)]
15. Pearton, S.; Kang, B.; Kim, S.; Ren, F.; Gila, B.; Abernathy, C.; Lin, J.; Chu, S. GaN-based diodes and transistors for chemical, gas, biological and pressure sensing. *J. Phys. Condens. Matter* **2004**, *16*, R961. [[CrossRef](#)]
16. Aliano, A.; Cicero, G.; Catellani, A. Origin of the accumulation layer at the InN/a-In₂O₃ interface. *ACS Appl. Mater. Interfaces* **2015**, *7*, 5415–5419. [[CrossRef](#)] [[PubMed](#)]
17. Liu, J.; Dai, M.; Wang, T.; Sun, P.; Liang, X.; Lu, G.; Shimanoe, K.; Yamazoe, N. Enhanced gas sensing properties of SnO₂ hollow spheres decorated with CeO₂ nanoparticles heterostructure composite materials. *ACS Appl. Mater. Interfaces* **2016**, *8*, 6669–6677. [[CrossRef](#)] [[PubMed](#)]
18. Sun, P.; Cai, Y.; Du, S.; Xu, X.; You, L.; Ma, J.; Liu, F.; Liang, X.; Sun, Y.; Lu, G. Hierarchical α-Fe₂O₃/SnO₂ semiconductor composites: Hydrothermal synthesis and gas sensing properties. *Sens. Actuators B Chem.* **2013**, *182*, 336–343. [[CrossRef](#)]
19. An, X.; Jimmy, C.Y.; Wang, Y.; Hu, Y.; Yu, X.; Zhang, G. WO₃ nanorods/graphene nanocomposites for high-efficiency visible-light-driven photocatalysis and NO₂ gas sensing. *J. Mater. Chem.* **2012**, *22*, 8525–8531. [[CrossRef](#)]
20. Tanaka, A.; Hashimoto, K.; Kominami, H. Visible-light-induced hydrogen and oxygen formation over Pt/Au/WO₃ photocatalyst utilizing two types of photoabsorption due to surface plasmon resonance and band-gap excitation. *J. Am. Chem. Soc.* **2014**, *136*, 586–589. [[CrossRef](#)] [[PubMed](#)]
21. Chen, D.; Ye, J. Hierarchical WO₃ hollow shells: Dendrite, sphere, dumbbell, and their photocatalytic properties. *Adv. Funct. Mater.* **2008**, *18*, 1922–1928. [[CrossRef](#)]
22. Li, X.-L.; Lou, T.-J.; Sun, X.-M.; Li, Y.-D. Highly sensitive WO₃ hollow-sphere gas sensors. *Inorg. Chem.* **2004**, *43*, 5442–5449. [[CrossRef](#)] [[PubMed](#)]
23. Penza, M.; Tagliente, M.; Mirengi, L.; Gerardi, C.; Martucci, C.; Cassano, G. Tungsten trioxide (WO₃) sputtered thin films for a NO_x gas sensor. *Sens. Actuators B Chem.* **1998**, *50*, 9–18. [[CrossRef](#)]
24. Lee, D.-S.; Han, S.-D.; Huh, J.-S.; Lee, D.-D. Nitrogen oxides-sensing characteristics of WO₃-based nanocrystalline thick film gas sensor. *Sens. Actuators B Chem.* **1999**, *60*, 57–63. [[CrossRef](#)]
25. Tao, W.-H.; Tsai, C.-H. H₂S sensing properties of noble metal doped WO₃ thin film sensor fabricated by micromachining. *Sens. Actuators B Chem.* **2002**, *81*, 237–247. [[CrossRef](#)]
26. Deng, L.; Ding, X.; Zeng, D.; Tian, S.; Li, H.; Xie, C. Visible-light activate mesoporous WO₃ sensors with enhanced formaldehyde-sensing property at room temperature. *Sens. Actuators B Chem.* **2012**, *163*, 260–266. [[CrossRef](#)]
27. Wang, G.; Ji, Y.; Huang, X.; Yang, X.; Gouma, P.-I.; Dudley, M. Fabrication and characterization of polycrystalline WO₃ nanofibers and their application for ammonia sensing. *J. Phys. Chem. B* **2006**, *110*, 23777–23782. [[CrossRef](#)] [[PubMed](#)]
28. Guruvenket, S.; Rao, G.M. Bias induced structural changes in tungsten nitride films deposited by unbalanced magnetron sputtering. *Mater. Sci. Eng. B* **2004**, *106*, 172–176. [[CrossRef](#)]
29. Li, G.; Song, J.; Pan, G.; Gao, X. Highly Pt-like electrocatalytic activity of transition metal nitrides for dye-sensitized solar cells. *Energy Environ. Sci.* **2011**, *4*, 1680–1683. [[CrossRef](#)]
30. Cui, S.; Pu, H.; Wells, S.A.; Wen, Z.; Mao, S.; Chang, J.; Hersam, M.C.; Chen, J. Ultrahigh sensitivity and layer-dependent sensing performance of phosphorene-based gas sensors. *Nat. Commun.* **2015**, *6*. [[CrossRef](#)] [[PubMed](#)]
31. Kulkarni, G.S.; Reddy, K.; Zhong, Z.; Fan, X. Graphene nanoelectronic heterodyne sensor for rapid and sensitive vapour detection. *Nat. Commun.* **2014**, *5*, 4376. [[CrossRef](#)] [[PubMed](#)]
32. Sun, Y.-F.; Liu, S.-B.; Meng, F.-L.; Liu, J.-Y.; Jin, Z.; Kong, L.-T.; Liu, J.-H. Metal oxide nanostructures and their gas sensing properties: A review. *Sensors* **2012**, *12*, 2610–2631. [[CrossRef](#)] [[PubMed](#)]
33. Ganbavle, V.; Inamdar, S.; Agawane, G.; Kim, J.; Rajpure, K. Synthesis of fast response, highly sensitive and selective Ni:ZnO based NO₂ sensor. *Chem. Eng. J.* **2016**, *286*, 36–47. [[CrossRef](#)]

34. Koziej, D.; Bârsan, N.; Weimar, U.; Szuber, J.; Shimanoe, K.; Yamazoe, N. Water–oxygen interplay on tin dioxide surface: Implication on gas sensing. *Chem. Phys. Lett.* **2005**, *410*, 321–323. [[CrossRef](#)]
35. Wang, C.; Li, X.; Feng, C.; Sun, Y.; Lu, G. Nanosheets assembled hierarchical flower-like WO₃ nanostructures: Synthesis, characterization, and their gas sensing properties. *Sens. Actuators B Chem.* **2015**, *210*, 75–81. [[CrossRef](#)]
36. Wang, L.; Dou, H.; Lou, Z.; Zhang, T. Encapsuled nanoreactors (Au@SnO₂): A new sensing material for chemical sensors. *Nanoscale* **2013**, *5*, 2686–2691. [[CrossRef](#)] [[PubMed](#)]
37. Bao, M.; Chen, Y.; Li, F.; Ma, J.; Lv, T.; Tang, Y.; Chen, L.; Xu, Z.; Wang, T. Plate-like p–n heterogeneous NiO/WO₃ nanocomposites for high performance room temperature NO₂ sensors. *Nanoscale* **2014**, *6*, 4063–4066. [[CrossRef](#)] [[PubMed](#)]
38. Nandi, D.K.; Sen, U.K.; Sinha, S.; Dhara, A.; Mitra, S.; Sarkar, S.K. Atomic layer deposited tungsten nitride thin films as a new lithium-ion battery anode. *Phys. Chem. Chem. Phys.* **2015**, *17*, 17445–17453. [[CrossRef](#)] [[PubMed](#)]



© 2016 by the authors; licensee MDPI, Basel, Switzerland. This article is an open access article distributed under the terms and conditions of the Creative Commons Attribution (CC-BY) license (<http://creativecommons.org/licenses/by/4.0/>).